Optical Coherence Tomography Angiography of a Choroidal Neovascularization in Adult Onset Foveomacular Vitelliform Dystrophy: Pearls and Pitfalls

Marco Lupidi,[1,2] Gabriel Coscas,[1,3] Carlo Cagini,[2] and Florence Coscas[1,3]

[1]Centre de l'Odéon, Paris, France
[2]Department of Biomedical and Surgical Sciences, Section of Ophthalmology, University of Perugia, S. Maria della Misericordia Hospital, Perugia, Italy
[3]Department of Ophthalmology, Centre Hospitalier Intercommunal de Créteil, Université Paris Est, Créteil, France

Correspondence: Gabriel Coscas, Centre Hospitalier Intercommunal de Créteil, 40 Avenue de Verdun, 94000 Créteil, France; gabriel.coscas@gmail.com.

PURPOSE. The purpose of this study was to determine the sensitivity and specificity of optical coherence tomography angiography (OCT-A) in detecting choroidal neovascularization (CNV)-complicating adult onset foveomacular vitelliform dystrophy (AOFVD) and to highlight the possible pitfalls related to the heterogeneous spectrum of acquired vitelliform maculopathies.

METHODS. Twenty-five eyes of 22 consecutive AOFVD patients with suspected CNV were enrolled. Conventional multimodal imaging findings, based on fluorescein angiography (FA), indocyanine green angiography (ICGA) and B-Scan OCT, were used as a basis and were compared with those obtained from OCT-A to define its sensitivity and specificity for detecting CNV in the case of AOFVD. A qualitative and quantitative analysis of the CNV appearance and of the associated OCT-A findings were also performed with the aim of defining features and elucidating possible diagnostic pitfalls.

RESULTS. Conventional multimodal imaging allowed diagnosis of a CNV in 5 of 25 eyes (20%), whereas a CNV lesion was clearly observed on OCT-A in 4 of 25 cases (16%). The sensitivity and specificity of CNV detection by OCT-A in cases of AOFVD was 4 of 5 cases (80%) and 20 of 20 cases (100%), respectively. Optical coherence tomography angiography in 10 cases (40%) showed a focal hyperintense signal, without vascular aspects, at the level of the outer nuclear layer or immediately above the subretinal material accumulation.

CONCLUSIONS. Our study demonstrates the capability of OCT-A to allow diagnosis of the presence of a CNV in AOFVD patients. Although FA remains the gold standard for determining the presence of a neovascular network, OCT-A offers noninvasive monitoring of the retinal and choroidal microvasculature, aiding in diagnosis and treatment decisions during follow-up.

Keywords: adult onset foveomacular vitelliform dystrophy, amplitude decorrelation angiography, choroidal neovascularization, CNV, multimodal imaging, OCT-A, OCT angiography

Adult-onset foveomacular vitelliform dystrophy (AOFVD) is a prevalent form of macular degeneration. When AOFVD was first described by Gass[1] in 1974, the phenotype was initially called "peculiar foveomacular dystrophy." It was later renamed AOFVD and has since been classified as one of several forms of pattern dystrophy.[2]

This condition typically occurs between the fourth and sixth decades of life, presenting with bilateral subfoveal yellowish deposits covering approximately one-third of the disc area with a central pigmented spot. Over time, the lesion's pigmentation may extend and become more intense, the yellow discoloration may diminish, and the retinal pigment epithelium (RPE) may develop atrophic regions.[3] In addition to the vitelliform lesion, consistent findings among these reports included various degrees of RPE hyperpigmentation, RPE detachment, presence of drusen in a subset of patients and choroidal neovascularization.[4–9]

Choroidal neovascularization (CNV) is a relatively uncommon complication of AOFVD, with an estimated rate of 11.7% after a 6-year follow-up.[9] The leading feature is the presence of abnormal blood vessels that originate from the choroid and extend mainly between Bruch's membrane and RPE type I or into the subretinal space RPE type II. Choroidal neovascularization proliferation can sometimes induce hemorrhages, fluid exudation, and fibrosis, resulting in severe photoreceptor damage and vision loss. Detection of CNV in AOFVD may alter clinical management; an early diagnosis is important to promptly treat CNV.[7]

Several imaging examination methods such as autofluorescence, fluorescein angiography (FA), indocyanine green angiography (ICGA), and spectral domain optical coherence tomography (SD-OCT) have led to a better understanding of the pathophysiological features of macular diseases.[10]

Fluorescein angiography is currently the method of choice for diagnosing and classifying CNV as a classic, occult, or

combination subtype, whereas ICGA can be used to identify the entire extension of the CNV lesion because of its ability to image the sub-RPE components of CNV.[10] Optical coherence tomography and, in particular, SD-OCT, with its high-resolution scanning capabilities, has revolutionized the diagnostic approach to exudative maculopathies. SD-OCT is able to define morphologic features of the fibrovascular complex as well as exudative consequences of fluid accumulation with retinal thickening and edema.[11]

A novel diagnostic technique, OCT angiography (OCT-A), allows a depth-resolved visualization of the retinal[12] and choroidal microvasculature.[13,14] Optical coherence tomography angiography is based on the concept that in a static eye, the only moving structure in the ocular fundus is the blood flowing in the vessels. A contrast is generated by differentiating between moving cells in the vasculature and the static surrounding tissue. By calculating the decorrelation of the signal amplitude from repeated consecutive B-scans in the same section, a contrast is generated between static and nonstatic tissue, resulting in a vascular decorrelation signal that enables the visualization of three-dimensional retinal and choroidal vascular structure.[13,14] Optical coherence tomography angiography does not require administration of an intravenous dye, such as fluorescein or indocyanine-green, thus avoiding potential risks that can result in nausea or other rare adverse events.[15,16]

In this study, we determined the capability of OCT-A to detect CNV lesions complicating AOFVD and highlighted the possible diagnostic pitfalls related to the heterogeneous spectrum of vitelliform maculopathies.

METHODS

Study Design

This observational cross-sectional retrospective study was conducted in the Odeon Ophthalmology Center (Paris, France). This study was performed in accordance with the Declaration of Helsinki after approval by the Paris Institutional Ethics Committee. Fully informed written consent was obtained from all study patients prior to scanning with the prototype OCT system.

Study Population

Twenty-five eyes of 22 consecutive patients with a clinical diagnosis of AOFVD underwent, in a random fashion on the same day, conventional multimodal imaging or OCT-A for the suspicion of active CNV, between November 2014 and March 2015.

Inclusion criteria were age older than 40 years old; complaint of visual impairment or metamorphopsias; round, yellowish, homogenous or heterogeneous macular lesions in the fundus examination; and hyperautofluorescence associated, or not, with a central polymorphic area of hyperpigmentation.

Exclusion criteria were any associated, previous, or concomitant ophthalmologic condition, such as media opacities, that could confound the interpretation of conventional multimodal imaging or OCT-A.

Conventional Multimodal Imaging

Each patient initially underwent a complete bilateral multimodal imaging protocol, including FA (in the absence of a clear contraindication to the use of dye injection), ICGA, and enhanced depth imaging SD-OCT (Heidelberg Retina Tomograph II + OCT; Spectralis; Heidelberg Engineering, Heidel-berg, Germany) to evaluate the presence of a CNV complicating the acquired vitelliform dystrophy.

Parameters recorded were presence or absence of staining in the late phase of FA, presence or absence of leakage from the lesion in late phase of FA, presence or absence of a neovascular network on ICGA, presence or absence of sub- or intraretinal optical empty space and heterogeneous (variable internal reflectivity) pigmented epithelium detachment on SD-OCT.

OCT-A

Study eyes were evaluated using an OCT-A prototype (based on Spectralis OCT2; Heidelberg Engineering) that was able to acquire 70,000 A-scans per second, each with a 7-μm axial and 14-μm lateral resolution. The ocular light power exposure was within the American National Standards Institute safety limit.[17] An amplitude decorrelation algorithm developed by the manufacturer was applied to a volume scan on a 15° × 5° area, composed of 131 B-scans (35 frames per scan) at a distance of 11 μm each.

In cases in which the 15° × 5° area showed an AOFVD that extended beyond the image border, a 15° × 10° OCT-A image (261 B-scans, 35 frames per scan) was used so that the entire lesion was evaluated.

Optical coherence tomography angiography was generated by computing the decorrelation between standard B-scans that were sequentially acquired at the same location. Decorrelation between each acquired B-scan and a second one taken in the same location was computed to obtain an OCT B-scan angiogram.

The C-scan ("en face") visualization of this OCT-A was automatically derived from the OCT B-scan angiograms mentioned above. The automated real-time mode combined with the narrow distance between two consecutive B-scans (11 μm) helped to diminish the signal-to-noise ratio. Moreover, the Active Eye tracking system of the OCT2 prototype (TruTrack; Heidelberg Engineering), which allowed the patient to rest in case of fatigue onset during the examination, provided the best high-resolution C-scan angiogram, even in cases of poor fixation or blinking.

Each OCT-A was simultaneously obtained along with the corresponding standard OCT B-scan; thus, both retinal and choroidal functions and morphologic images were acquired. Optical coherence tomography angiography software (Heyex software version 1.9.201.0; Heidelberg Engineering) provided an automated segmentation algorithm for the retinal and choroidal layers. In case of eventual segmentation errors due to accentuated macular retinal or choroidal changes, a manual correction of the alignment was allowed.

Two automatically segmented lines separated by 30 μm, which were horizontal or shaped on the RPE profile, were manually fine tuned to be located at the level of the external boundary of the outer plexiform layer and then moved progressively deeper in 30-μm steps to the choroid-sclera interface. This procedure allowed for the analysis of all structures included in a 30-μm–thick slice of tissue in an en-face visualization. The 30-μm thickness was established for each C-scan because it showed all coplanar structures in a given section while avoiding the risk of superimposition typical of thicker sections. The possibility of having an RPE-shaped C-scan section enables clear visualization of the neovascular tissue attached to the back surface of the RPE.[18]

The importance of starting the assessment at the level of the external boundary of the outer plexiform layer lies in the fact that there are no vascular structures in healthy eyes at this level. Therefore, OCT-A is not expected to detect blood flow at the depth of the outer retinal layers.

Simultaneously available standard OCT B-scans and C-scans provided useful information for identifying the specific anatomical level of each analyzed OCT-A C-scan and provided indications about the presence of possible neovascular activity, such as subretinal fluid or intraretinal cystoid spaces.

Choroidal neovascularization presence on OCT-A was defined by evidence of a hyperintense decorrelation signal immediately above the RPE (CNV type II) and/or below the RPE (CNV type I) between Bruch's membrane and the RPE layers.

The OCT-A C-scan images were assessed for CNV appearance and size. The appearance of CNV on the OCT-A image was described in accordance with a previously reported methodology.[14,19,20]

Choroidal neovascularization size was evaluated using the greatest linear dimension (GLD) and area. Optical coherence tomography angiography automated software included tools for the measurement of GLD and lesion area. Choroidal neovascularization area was computed by manually outlining the border of the neovascular lesion. The automated software provided corresponding values in square millimeters. A similar process was used to obtain the GLD. Moreover, every type of focal hyperintense decorrelation signal at the level of the outer retina was registered and evaluated.

Comparative Imaging Analysis

All evaluations were performed by two retinal specialists (ML, FC), who were masked to each other's evaluations and independently graded the images obtained from the conventional multimodal and OCT-A protocols at different time points and in different orders. Results obtained for each imaging protocol by the two different assessors were then compared and, in the case of discordance, were further analyzed by a senior retinal specialist (GC).

Conventional multimodal imaging was then used as the basis to calculate the sensitivity and specificity of OCT-A in detecting CNV. If an eye was determined to have CNV on conventional multimodal imaging, the OCT-A image was considered to be a true positive if a CNV was observed or a false negative if a CNV was not visualized. Conversely, if the conventional multimodal imaging did not show a CNV, the OCT-A image was considered a true negative if no CNV was observed or a false positive if a CNV was considered present.

A simple Kappa coefficient was used to assess the interimaging methodology agreement on CNV detection in AOFVD. SAS version 9.3 software (SAS, Cary, NC, USA) was used for statistical calculations.

RESULTS

Study Population

Twenty-five eyes of 22 consecutive AOFVD patients were enrolled in this study. All were caucasians with a mean ± SD age of 70.1 ± 10.5 years. There were 13 females (59.1%). All patients underwent FA, ICGA, SD-OCT, and OCT-A examinations. No adverse effects related to the procedures (i.e., dye injections) were reported. In 3 of 25 cases, the scanning area on OCT-A was increased from 15° × 5° (131 B-scans) to 15° × 10° (261 B-scans) because the AOFVD lesion extended beyond the image border. Mean acquisition time for OCT-A examination was 90 seconds (range, 60–120 seconds).

Conventional Multimodal Imaging Analysis

FA showed the presence of late staining of the lesion in all 25 eyes (100%); leakage was detected in 4 eyes (16%), and there was no leakage in the remaining eyes. Indocyanine green angiography showed the presence of a CNV network in 5 of the 25 study eyes. Sub- or intraretinal optical empty spaces were diagnosed on SD-OCT in 17 eyes (68%), with no sub- or intraretinal optical empty spaces in the remaining eyes. A heterogeneous pigmented epithelium detachment (PED) was observed in 5 eyes (20%), with no heterogeneous PED in the rest.

In the final computation, the conventional multimodal imaging approach assisted in diagnosis of a CNV in 5 of 25 eyes (20%), whereas a CNV was determined to be absent in the other 20 examined cases.

OCT-A Imaging Analysis

A CNV lesion was clearly observed on OCT-A in 4 of 25 study eyes (16%). Of the four cases with CNV detected by OCT-A, the shape of the neovascular lesion was defined as shaped like a "lacy wheel" or "sea fan" in three eyes (75%), and the remaining lesions (25%) were characterized by long filamentous linear vessels. In all cases, the vessel's caliber was relatively homogeneous from the center to the periphery of the lesions, with a limited number of anastomoses and rarely the presence of peripheral arcades at the vessels' termini.

Quantitative assessment of the choroidal neovascular networks showed a mean GLD of 1152 μm (range, 727–1931 μm; median: 975 μm) and an average CNV area of 0.87 mm^2 (range, 0.32–2.34 mm^2; median: 0.4 mm^2).

In 10 cases (40%), a focal hyperintense signal without vascular appearance (i.e., no "sea-fan" or "lacy wheel" shape nor sinuous vessels) was shown on OCT-A at the level of the outer nuclear layer or immediately above the subretinal material accumulation.

Comparative Analysis

Conventional multimodal imaging and OCT-A diagnoses were established by an independent evaluation by two trained readers at the Odeon Ophthalmology Center. There was high ($P < 0.05$) interobserver agreement for CNV detection in both conventional multimodal and OCT-A imaging analyses. A simple κ coefficient was used to assess interimaging methodology agreement on CNV detection in AOFVD and was 0.86 (95% confidence interval: 0.61–1).

Figure 1 shows the conventional multimodal imaging (Figs. 1A, 1B, 1C) and OCT-A (Figs. 1D, 1E, 1F) images from a 46-year-old white male with AOFVD and a doubtful secondary CNV in the left eye. The FA image (Fig. 1A) demonstrated in the late phase the presence of an irregularly stained central lesion with some weak leakage mainly from the nasal borders. The ICGA (Fig. 1B) during the venous phase showed the presence of a hyperfluorescent lesion in the foveal area. SD-OCT (Fig. 1C) showed a dome-shaped subretinal lesion in the vitelliform stage. The content of the lesion was homogenously hyperreflective. The 30-μm–thick OCT-A C-scan (Fig. 1D), passing through the lesion (Figs. 1E, 1F), illustrated a well-circumscribed CNV in the subfoveal area, with the typical "spoked-wheel" shape, several large central vessels branching into smaller ones toward the periphery, and some anastomoses and loops. On the OCT-A B-scan (Fig. 1E), an evident decorrelation signal coming from various structures was visible. Multiple hyperintense microdots in the retina, representing the superficial capillary plexus and the deep capillary plexus, were detected in the ganglion cell layer and the inner nuclear layer, respectively. A hyperintense signal coming from the choroidal vasculature (choriocapillaris [Sattler and Haller layers]) was also shown. Moreover, a pathologic hyperintense signal (due to the presence of perfused new vessels) was
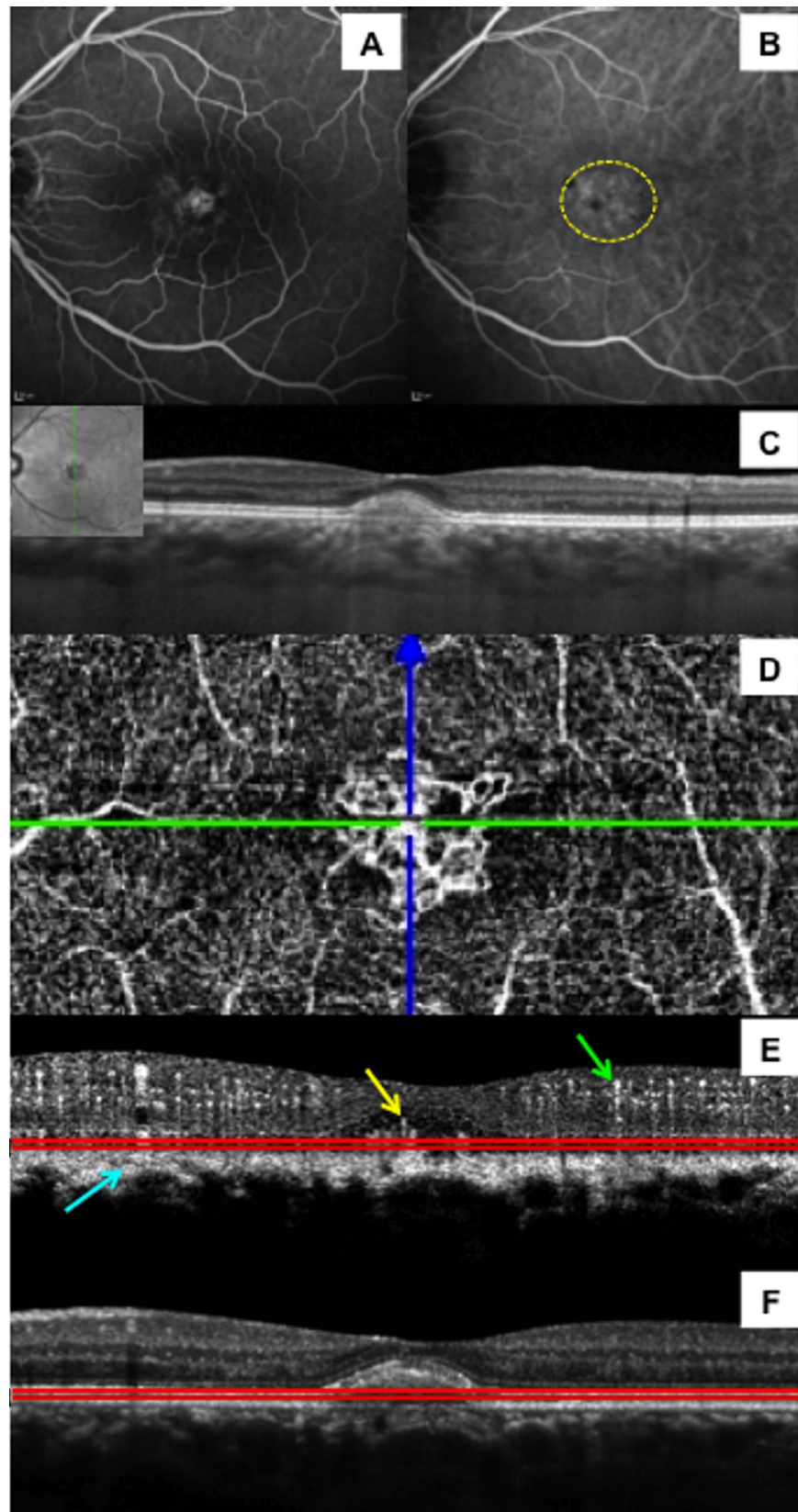
FIGURE 1. Conventional multimodal imaging (**A–C**) and OCT-A (**D–F**) images from a 46-year-old white man with AOFVD and a suspected secondary CNV in the left eye. (**A**) Late phase FA image demonstrating the presence of an irregularly stained central lesion with some weak leakage at the nasal borders. (**B**) Indocyanine green angiography during the venous phase showing the presence of a hyperfluorescent lesion in the foveal area (*yellow dashed line*). (**C**) Spectral-domain OCT showing a dome-shaped subretinal lesion in the vitelliform stage. The content of the lesion is homogenously hyper-reflective. (**D**) A 30-μm–thick OCT-A C-scan of an area 15° × 5° passing through the lesion, illustrating a well-circumscribed CNV in subfoveal area, with the typical "spoked-wheel" shape, several large central vessels branching into smaller vessels toward the periphery, and some

anastomoses and loops. Artifacts from retinal vessels are also visible at the scanned level. (**E**) Optical coherence tomography angiography B-scan showing an evident decorrelation signal coming from various structures. Multiple hyperintense microdots in the inner retinal layers (*green arrow*) representing the superficial capillary plexus and the deep capillary plexus are detected in ganglion cell and inner nuclear layers, respectively. A hyperintense signal coming from the choroidal vasculature (choriocapillaris [Sattler and Haller layers]) is also shown (*cyan arrow*). Moreover, a pathologic hyperintense signal is present in the lesion area (*yellow arrow*) starting above the reference plan (*red line*) of the previously described C-scan (**D**). (**F**) Corresponding coregistered conventional OCT B-scan showing the vitelliform subretinal lesion and the reference plan (*red lines*) of the OCT-A C-scan (**D**).

evident in the lesion area; some tiny hyperintense structures were visible above the reference plan (red lines) of the previously described C-scan.

Among the five cases with CNV detected by conventional multimodal imaging, four cases were also found to have CNV by using OCT-A. The sensitivity of CNV detection by OCT-A was therefore four of five (80%).

Figure 2 shows conventional multimodal imaging (Figs. 2A, 2B, 2C) and OCT-A (Figs. 2D, 2E, 2F) images from a 74-year-old white female with AOFVD and doubtful secondary CNV in the right eye. The FA image (Fig. 2A) demonstrates in the late phase the presence of an irregular weak hyperfluorescence in the macular area. The ICGA (Fig. 2B) during the venous phase shows the presence of a hypofluorescent lesion in the macular area due to the masking effect of the subretinal material accumulation, without any evidence of a neovascular network. SD-OCT (Fig. 2C) demonstrated a dome-shaped subretinal lesion in the vitelliform stage. The content of the lesion was hyper-reflective with discrete pigmented epithelium detachment. The 30-μm–thick OCT-A C-scan (Fig. 2D) and corresponding OCT-A B-scan (Fig. 2E) did not show any hyperintense decorrelation signal that could be due to a CNV presence in the subfoveal area. The OCT-A C-scan showed a grayish, round lesion of relatively homogeneous signal intensity with no evidence of perfused (hyperintense) structures inside that blocked the reflected image of retinal vessels, which is normally present at the outer retina.[19]

Of the 20 images without CNV on conventional multimodal imaging, all 20 were also determined to have no CNV on OCT-A. Therefore, the specificity of CNV detection by OCT-A was 20 of 20 (100%).

DISCUSSION

Dye angiography is critical for the initial diagnosis of choroidal neovascularization.[21–23] Spectral-domain OCT, although indispensable in clinical management due to its capability to assess the activity of the lesion, cannot identify either the CNV structure or its perfusion because the reflectivity of the CNV is similar to that of drusen, hemorrhage, fibrosis, and changes in the outer retinal layer.[24]

The present study shows the high sensitivity (4 of 5 [80%]) and specificity (20 of 20 [100%]) of the Spectralis OCT-A prototype in detecting a CNV lesion in AOFVD patients. This result is consistent with that of previous studies in which, although different devices (e.g., swept-source OCT) and different decorrelation algorithms (e.g., split-spectrum amplitude decorrelation angiography) were used, the sensitivity in detecting choroidal neovascular lesions ranged from 50% to 100% in the case of exudative age-related macular degeneration[13,14,25] or was equal to 100% in the case of central serous chorioretinopathy.[26]

The single false negative OCT-A image showed a lesion that was identified on conventional multimodal imaging as a type 3 choroidal neovascularization (retinal angiomatous proliferation) and was determined to show negative results. This result could be partially explained by the OCT-A analysis that, in the study protocol, included all retinal and choroidal layers between the outer plexiform and choroid-sclera interface, without evaluation of the retinal vascular layers. The latter might have provided some useful information on OCT-A for guiding the examiners to the correct diagnosis, although a type 3 CNV was unexpected in the case of AOFVD because it is generally associated with type 1 (or type 2) neovascularization.[7–9] Similar pitfalls have already been reported in a recent study by De Carlo et al.[14]; false negative cases were due to the presence of massive subretinal hemorrhage (which could block the OCT signal), the localization of the CNV, or motion artifacts.

Various qualitative aspects of the choroidal neovascular lesions identified on OCT-A were reported. Three of four CNVs showed a "lacy wheel" or "sea fan" aspect, and only one case presented long filamentous vessels. Moreover, that vessel's calibers appeared to be relatively homogeneous in the entire lesion in all cases, as well as have a limited number of anastomoses and tiny peripheral arcades at the vessels' termini. This new nomenclature, which is rapidly spreading,[13,14,19,20] has introduced a new descriptive approach of the neovascular lesion. Although it is waiting for a statistical validation, various aspects of neovascularization might correspond with various stages of activity. The present study results, which revealed the small size of the lesions and lack of qualitative features that are potentially attributable to active proliferation (tiny branches, anastomoses and peripheral arcades), only speculate about the quiescence or limited activity of the CNV.

Nevertheless, it is extremely important that the entire thickness of a CNV lesion, if detected, is thoroughly analyzed to qualitatively define a choroidal neovascular network. Optical coherence tomography angiography provides depth-resolved images, and therefore, manual adjustment of the segmentation and C-scan level from the outer retinal boundaries to the deep choroid was required to allow a layer-by-layer tomographic visualization of the entire neovascular network. In fact, because CNV is not a coplanar structure, it could show various features and patterns at various depths when imaged by OCT-A. Therefore, all C-scan sections (30 μm per step) showing an evident decorrelation signal related to the CNV were evaluated in detail to have a complete qualitative assessment of the lesion.

The readers evaluating the OCT-A in this study were highly trained and performed a dynamic OCT-A volume analysis, with manual modifications of the segmentation lines if required. Such an evaluation aims to increase the sensitivity and specificity of the CNV evaluation on OCT-A because automated segmentation is often incorrect in the presence of severe disruption of the outer retinal layers.

The typical C-scan OCT-A of a vitelliform accumulation, without clear signs of CNV, showed a grayish, round lesion, more or less homogeneous, that blocked the reflected image of retinal vessels in the involved area. It has already been demonstrated that sections, including the RPE, may show artifacts from the retinal vessels, although the sections did not include the retinal vessels. This result is caused by temporally changing patterns of light passing through blood vessels that can be reflected from deeper structures such as the RPE.[19] The optical density of the vitelliform accumulation is able to block reflective abilities of the RPE, thereby preventing the pseudovisualization of the retinal vessels at the level of the outer retina.
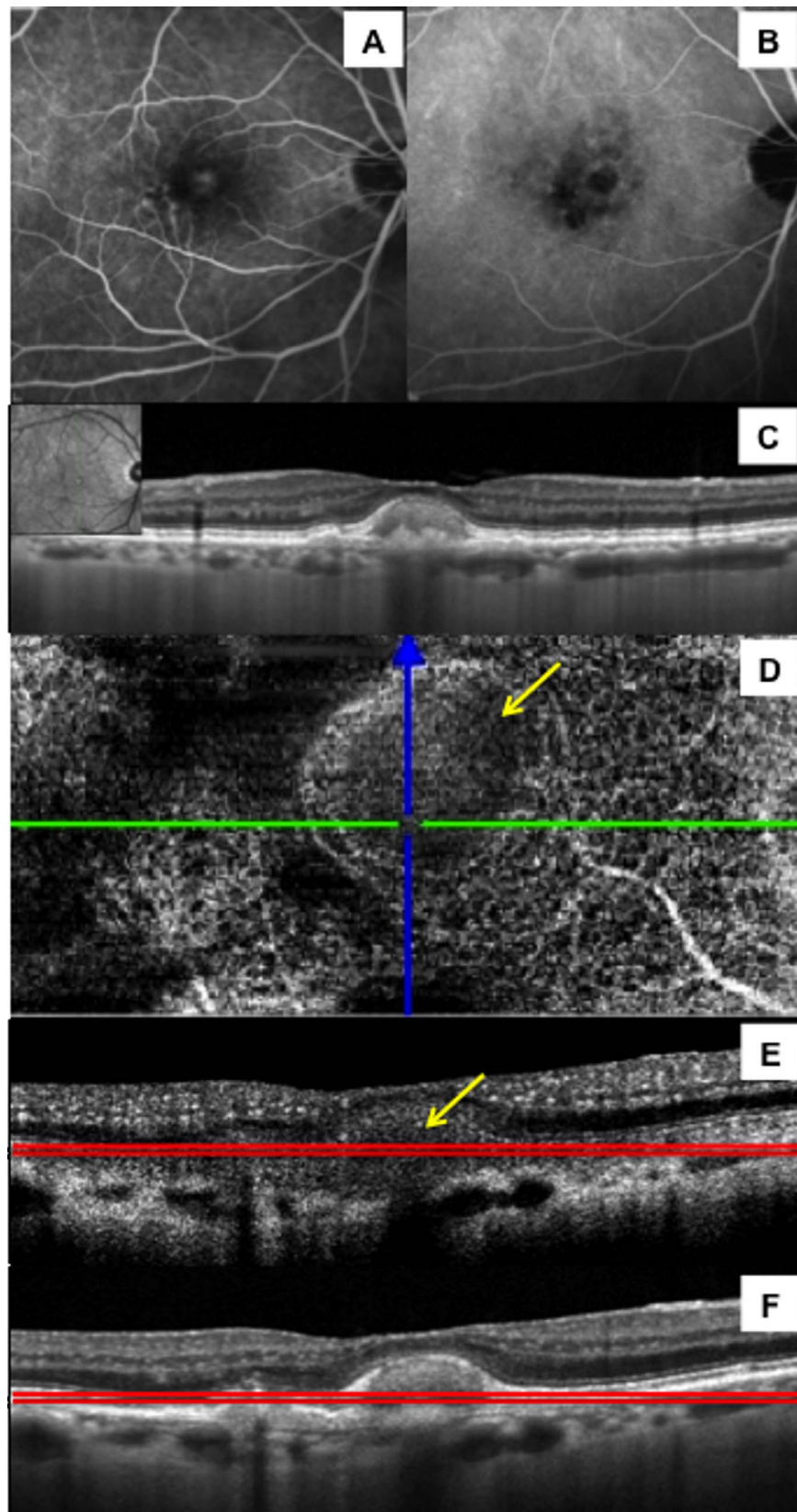
FIGURE 2. Conventional multimodal (A–C) and OCT-A (D–F) images from a 74-year-old white woman with AOFVD and a question of secondary CNV in the right eye. (A) Late phase FA image shows the presence of an irregular, weak hyperfluorescence in the macular area. (B) Indocyanine green angiography during the venous phase shows the presence of hypofluorescent lesions in the macular area due to the masking effect of subretinal material accumulation without evidence of a neovascular network. (C) Spectral-domain OCT shows a dome-shaped subretinal lesion in the vitelliform stage. The content of the lesion was hyper-reflective with discrete pigmented epithelium detachment. (D) A 30-μm–thick OCT-A C-scan and corresponding OCT-A B-scan (E) did not show any hyperintense decorrelation signal due to a CNV in the lesion area (*yellow arrows*). The

OCT-A C-scan (**D**) shows a grayish roundish lesion (*yellow arrow*) of relatively homogeneous signal intensity with no evidence of perfused (hyperintense) structures inside that is blocking the artifact from the retinal vessels, which is appreciable in the perilesional area. (**F**) Corresponding coregistered conventional OCT B-scan showing the vitelliform subfoveal lesion and the reference plan (*red lines*) of the OCT-A C-scan (**D**).

Optical coherence tomography angiography imaging analysis reported the presence of a hyperintense signal in 40% of eyes, without vascular appearance at the level of the outer nuclear layer or immediately above the subretinal material accumulation. By comparing the single OCT-A B-scan with its corresponding conventional B-scan (as perfectly coregistered), it became clear that the focal hyperintense signals corresponded to hyper-reflective clumps within the outer plexiform and outer nuclear layers, potentially representing pigment migration from the lesion area.[27] Moreover, further analysis of the OCT-A B-scan highlighted the fact that the hyperintense signal due to intraretinal clumps was associated with dark back-shadowing, as in conventional OCT; in contrast, a hyperintense signal due to a perfused structure (i.e., CNV) was sometimes associated with a hyperintense (bright) back tail, but did not

show any dark back shadowing (Fig. 3). We hypothesized, therefore, that intraretinal pigment clumps, which appear as highly hyperreflective structures on conventional OCT, might be hyperintense on OCT-A because of reflection of the light passing through the blood vessels above.

This particular finding, obtained from a simultaneous analysis of the C-scan and the B-scan on OCT-A, which was available on the Spectralis automated software, could help to avoid some pitfalls and guide the differential diagnosis.

The present study included a limited number of patients, the use of a prototype device, and the mainly qualitative evaluation of OCT-A and multimodal imaging findings, which, although conducted in a masked fashion, could suffer from the subjective nature of the assessment. Dye-based angiography provides dynamic information (transit time of dye to
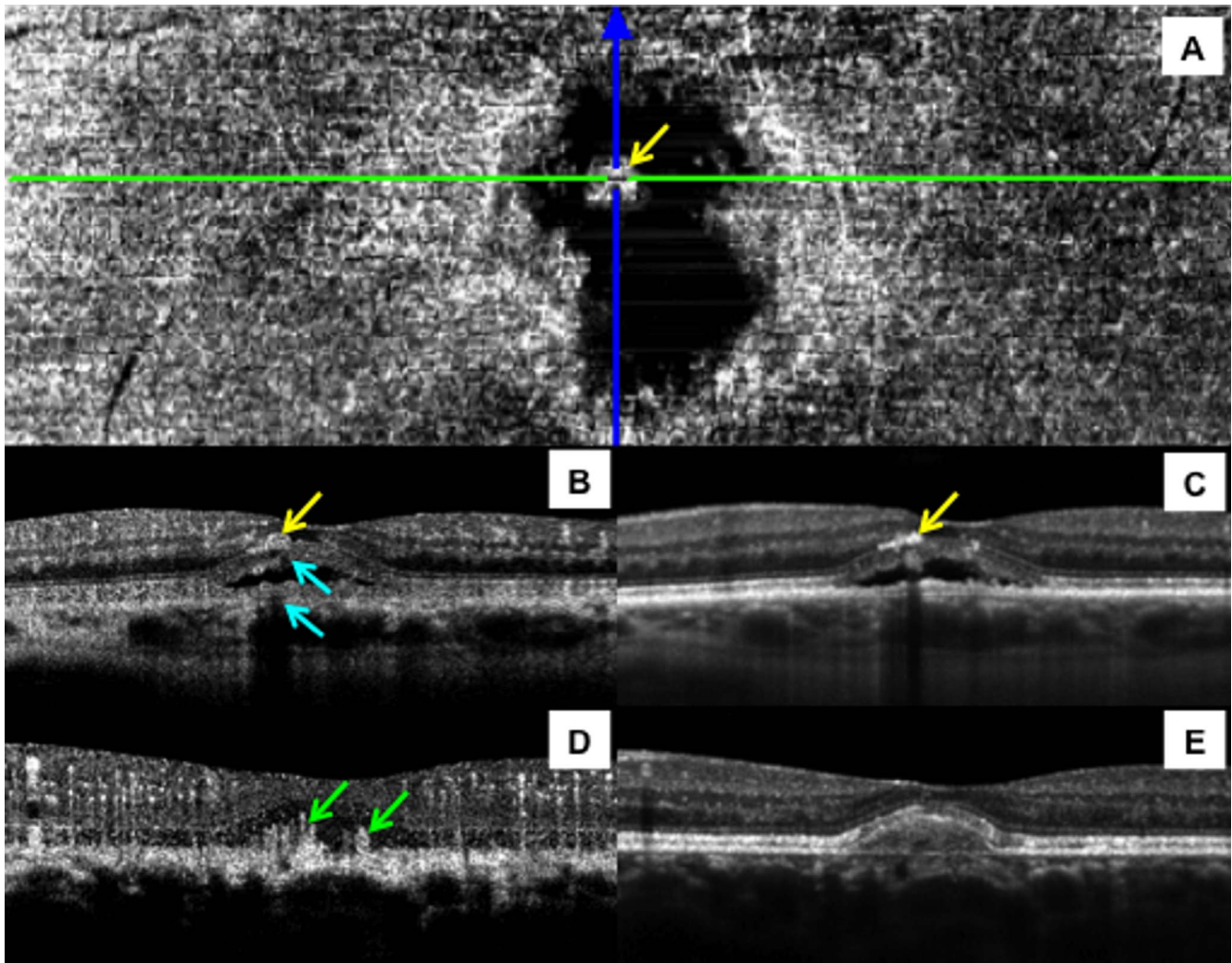

FIGURE 3. Differential diagnosis of hyperintense signals on OCT-angiography. (**A**) Optical coherence tomography angiography C-scan taken at the level of a vitelliform lesion (pseudohypopyon stage) presenting a focal hyperintense structure (*yellow arrow*) inside the lesion area. (**B**) Corresponding OCT-A B-scan shows the focal hyperintense structure in the foveal area (*yellow arrow*) immediately above a neuroretinal detachment associated with dark back-shadowing (*cyan arrows*). (**C**) Coregistered conventional OCT B-scan shows that the hyperintense OCT-A signal was due to intraretinal hyper-reflective clumps, probably caused by pigment migration. (**D**) Optical coherence tomography angiography B-scan of a neovascularization complicating a case of AOFVD. No dark back-shadowing of the new vessels is shown (*green arrows*). (**E**) Corresponding coregistered (**D**) conventional OCT B-scan shows a homogeneously hyper-reflective vitelliform subretinal lesion.

travel to the eye), which is currently not available on OCT-A. Moreover, the typical angiographic patterns assessing the presence and activity of retinal diseases, such as leakage, staining or pooling, are not visible on OCT-A. Finally, the scanning area is substantially limited in comparison with the new "wide field" devices that allow angiographic examination on more than a 100° area.

In conclusion, we have demonstrated the high sensitivity and specificity of OCT-A in detecting CNV in the case of AOFVD. Performing a careful segmentation or identifying the presence or absence of back-shadowing could help to avoid some potential pitfalls in this new diagnostic approach. Our study suggests that OCT-A is a useful technology for the non-invasive monitoring of the AOFVD because both functional and morphologic information are available from a single OCT scan. Such monitoring may help in diagnosing CNV, monitoring the evolution and possibly guiding treatment decisions.

References

1. Gass J. A clinicopathologic study of a peculiar foveomacular dystrophy. *Trans Am Ophthalmol Soc*. 1974;72:139–156.

2. Freund KB, Laud K, Lima LH, et al. Acquired vitelliform lesions: correlation of clinical findings and multiple imaging analyses. *Retina*. 2011;31:13–25.

3. Chowers I, Tiosano L, Audo I, et al. Adult-onset foveomacular vitelliform dystrophy: a fresh perspective. *Prog Retin Eye Res*. 2015;47:64–85.

4. Glacet-Bernard A, Soubrane G, Coscas G. Macular vitelliform degeneration in adults. Retrospective study of a series of 85 patients. *J Fr Ophtalmol*. 1990;13:407–420.

5. Spaide RF, Noble K, Morgan A, et al. Vitelliform macular dystrophy. *Ophthalmology*. 2006;113:1392–1400.

6. Querques G, Regenbohen M, Quijano C, et al. High-definition optical coherence tomography features in vitelliform macular dystrophy. *Am J Ophthalmol*. 2008;146:501–507.

7. Mimoun G, Caillaux V, Querques G, et al. Ranibizumab for choroidal neovascularization associated with adult-onset foveomacular vitelliform dystrophy: one-year results. *Retina*. 2013;33:513–521.

8. Coscas F, Puche N, Coscas G, et al. Comparison of macular choroidal thickness in adult onset foveomacular vitelliform dystrophy and age-related macular degeneration. *Invest Ophthalmol Vis Sci*. 2014;55:64–69.

9. Da Pozzo S, Parodi MB, Toto L, et al. Occult choroidal neovascularization in adult-onset foveomacular vitelliform dystrophy. *Ophthalmologica*. 2001;215:412–414.

10. Sulzbacher F, Kiss C, Munk M, et al. Diagnostic evaluation of type 2 (classic) choroidal neovascularization: optical coher-

11. Coscas G, Coscas F, Vismara S, et al. *Optical Coherence Tomography in AMD*. 1st ed. Heidelberg, Germany. Springer;2009:159–166.

12. Spaide RF, Klancnik JM Jr, Cooney MJ. Retinal vascular layers imaged by fluorescein angiography and optical coherence tomography angiography. *JAMA Ophthalmol*. 2015;133:45–50.

13. Jia Y, Bailey ST, Wilson DJ, et al. Quantitative optical coherence tomography angiography of choroidal neovascularization in age-related macular degeneration. *Ophthalmology*. 2014;121:1435–1444.

14. De Carlo TE, Bonini Filho MA, Chin AT, et al. Spectral-domain optical coherence tomography angiography of choroidal neovascularization. *Ophthalmology*. 2015;122:1228–1238.

15. Yannuzzi LA, Rohrer KT, Tindel LJ, et al. Fluorescein angiography complication survey. *Ophthalmology*. 1986;93:611–617.

16. Su Z, Ye P, Teng Y, et al. Adverse reaction in patients with drug allergy history after simultaneous intravenous fundus fluorescein angiography and indocyanine green angiography. *J Ocul Pharmacol Ther*. 2012;28:410–413.

17. *American National Standard for Safe Use of Lasers*: ANSI Z136. Orlando, FL: Laser Institute of America; 2007.

18. Coscas F, Coscas G, Souied E, et al. Optical coherence tomography identification of occult choroidal neovascularization in age-related macular degeneration. *Am J Ophthalmol*. 2007;144:592–599.

19. Spaide RF. Optical coherence tomography angiography signs of vascular abnormalization with antiangiogenic therapy for choroidal neovascularization. *Am J Ophthalmol*. 2015;160:6–16.

20. Coscas G, Lupidi M, Coscas F. *Atlas of OCT-Angiography in AMD*. Paris, France: L'Europeenne Editions; 2015:43–48.

21. Gass JD. Pathogenesis of disciform detachment of the neuroepithelium. *Am J Ophthalmol*. 1967;63(suppl):1–139.

22. Hyvärinen L, Flower RW. Indocyanine green fluorescence angiography. *Acta Ophthalmol (Copenh)*. 1980;58:528–538.

23. Do DV. Detection of new-onset choroidal neovascularization. *Curr Opin Ophthalmol*. 2013;24:244–247.

24. Giovannini A, Amato GP, Mariotti C, et al. OCT imaging of choroidal neovascularization and its role in the determination of patients' eligibility for surgery. *Br J Ophthalmol*. 1999;83:438–442.

25. Moult E, Choi W, Waheed NK, et al. Ultrahigh-speed swept-source OCT angiography in exudative AMD. *Ophthalmic Surg Lasers Imaging Retina*. 2014;45:496–505.

26. Bonini Filho MA, de Carlo TE, Ferrara D, et al. Association of choroidal neovascularization and central serous chorioretinopathy with optical coherence tomography angiography. *JAMA Ophthalmol*. 2015;133:899–906.

27. Puche N, Querques G, Blanco-Garavito R, et al. En face enhanced depth imaging optical coherence tomography features in adult onset foveomacular vitelliform dystrophy. *Graefes Arch Clin Exp Ophthalmol*. 2014;252:555–562.